Biophysical Society

Mechanically Regulated Outside-In Activation of an I-Domain-Containing Integrin

Debin Mao,[1,2] Shouqin Lü,[1,2,*] Xiao Zhang,[1,2] and Mian Long[1,2,*]
[1]Center of Biomechanics and Bioengineering, Key Laboratory of Microgravity (National Microgravity Laboratory), Beijing Key Laboratory of Engineered Construction and Mechanobiology, and CAS Center for Excellence in Complex System Mechanics, Institute of Mechanics, Chinese Academy of Sciences, Beijing, China and [2]School of Engineering Science, University of Chinese Academy of Sciences, Beijing, China

ABSTRACT Integrins are heterodimeric transmembrane proteins that mediate cellular adhesion and bidirectional mechanotransductions through their conformational allostery. The allosteric pathway of an I-domain-containing integrin remains unclear because of its complexity and lack of effective experiments. For a typical I-domain-containing integrin $\alpha_X\beta_2$, molecular dynamics simulations were employed here to investigate the conformational dynamics in the first two steps of outside-in activation, the bindings of both the external and internal ligands. Results showed that the internal ligand binding is a prerequisite to the allosteric transmission from the α- to β-subunits and the exertion of external force to integrin-ligand complex. The opening state of αI domain with downward movement and lower half unfolding of α_7-helix ensures the stable intersubunit conformational transmission through external ligand binding first and internal ligand binding later. Reverse binding order induces a, to our knowledge, novel but unstable swingout of β-subunit Hybrid domain with the retained close states of both αI and βI domains. Prebinding of external ligand greatly facilitates the following internal ligand binding and vice versa. These simulations furthered the understanding in the outside-in activation of I-domain-containing integrins from the viewpoint of internal allosteric pathways.

SIGNIFICANCE Allostery is a key feature for proteins and plays a pivotal role in the related biological functions. The allosteric pathways of heterodimeric transmembrane integrins are critical to mediate the bidirectional (inside-out and outside-in) mechanotransduction but still not fully understood because of their complexity and lack of effective measurements. Using molecular dynamics simulations, this study illustrated the chained conformational transmissions in a typical I-domain-containing integrin $\alpha_X\beta_2$ and demonstrated distinct contributions of external and internal ligand bindings and their cooperation to mechanical outside-in activation. These results elaborated the understanding in the outside-in activation of I-domain-containing integrins with conformational dynamics and allosteric pathways.

INTRODUCTION

Integrins are heterodimeric transmembrane proteins that mediate cellular adhesion and bidirectional mechanotransductions between extracellular ligands and actin cytoskeleton through adopting favorable conformations to implement various functions. For example, the intermediate-affinity (IA) state lymphocyte function-associated antigen-1 (CD11aCD18 or $\alpha_L\beta_2$) supports slow rolling of leukocyte on endothelial cells, and the high-affinity (HA) state one mediates leukocyte firm adhesion during inflammatory cascade (1–3). Thus, the allosteric dynamics of integrins are key to understand and elucidate their biological

functions. There exist 24 members of integrin family assembled by 18 α-subunits and eight β-subunits. Each β-subunit contains eight extracellular domains, that is, I-like (βI in brief), Hybrid, plexin-semaphorin-integrin, epidermal growth factor (EGF)-1–4, and β-tail domain, counting from the membrane distal end. All the 18 α-subunits contain four extracellular domains of β-propeller, Thigh, Calf-1, and Calf-2, counting from the membrane distal end, and half of them has an additional I domain (αI in brief) of 180–190 residues with its N- and C-terminals inserted into the β-propeller domain (4,5). The overall configuration of integrin ectodomains displays a large head supported by two long legs. The head of αI-domain-containing integrins consists of αI and β-propeller domains of the α-subunit and βI domain of the β-subunit (Fig. 1 A). The two legs contain the upper legs, including α-subunit Thigh domain and β-subunit Hybrid, plexin-semaphorin-integrin, and EGF-1
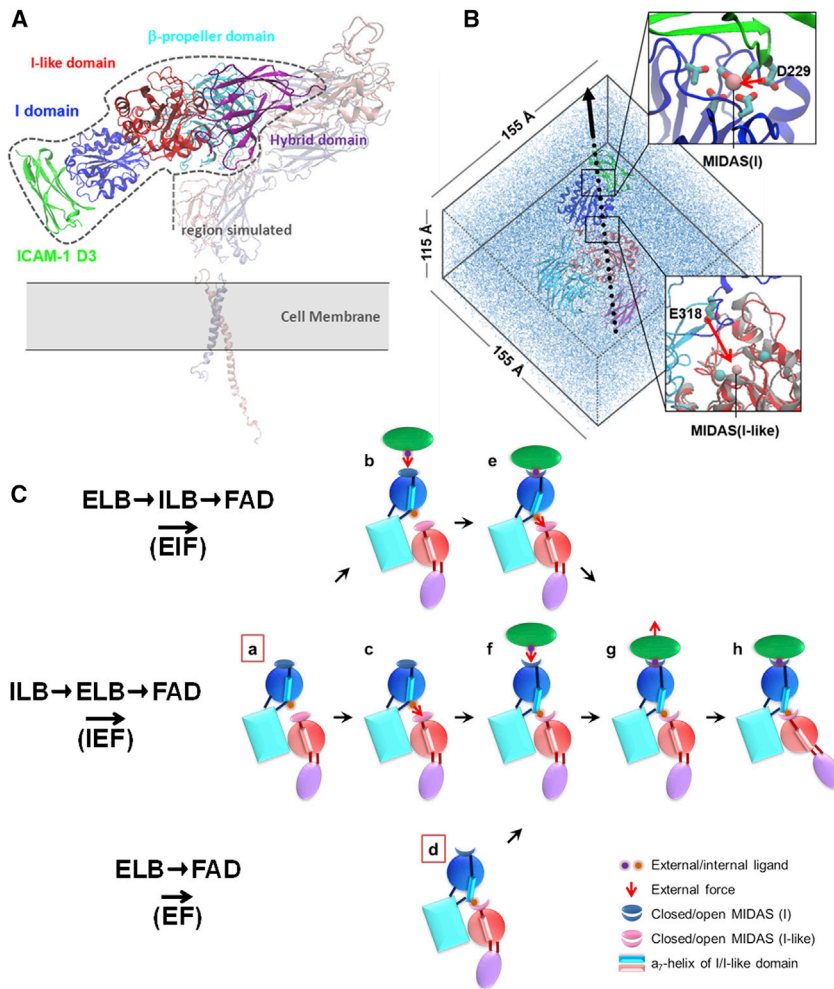
FIGURE 1 Design of MD simulations. (*A*) Ectodomain crystal structure of the $\alpha_X\beta_2$ integrin with schematic transmembrane regions and docked ligand of ICAM-1 D3 domain in newcartoon presentation. The domains included in the simulation system were drawn in opaque with the ICAM-1 D3 domain in green, I domain in blue, I-like domain in red, β-propeller domain in cyan, and Hybrid domain in purple. The other domains were shown in transparent. (*B*) Simulation system setup. The target domains of the $\alpha_X\beta_2$ integrin and ligand of ICAM-1 D3 domain were solvated in a quadrate water box for equilibration and forced binding or unbinding simulations. The red arrows in two zoomed regions indicated forces for external (*upper*) and internal (*lower*) ligand bindings, respectively. The black arrow in the left water box denoted the force for ligand unbinding. Ions were presented in vdW, with Mg^{2+} in pink and Ca^{2+} in cyan, and the key residues were shown in name licorice. (*C*) Three sets of simulation designs. Two sets of sequential simulations based on the crystal structure of 3K6S were named $\overrightarrow{EIF}$ and $\overrightarrow{IEF}$ (boxed *Ca*), and the other one based on 4NEH-4NEN as $\overrightarrow{EF}$ (boxed *Cd*). The detailed simulation processes for each set were demonstrated by sequential schematics. ELB, external ligand binding; FAD, force-induced allostery or dissociation; ILB, internal ligand binding. To see this figure in color, go online.

domains and the lower legs including α-subunit Calf-1 and -2 domains, β-subunit EGF-2–4 domains, and β-tail domains. Both head and upper legs together are often named as headpiece and the lower legs as tailpiece.

Three global conformational states of bent closed, extended closed, and extended open have been previously reported for several integrin members, which bind to the corresponding ligand with low-affinity (LA), intermediate affinity (IA), and high affinity (HA), respectively (6–11). These distinct conformations of integrins are accompanied by the coordinated arrangements of both α- and β-subunit domains and the conformational adjustments of the domains themselves. Importantly, switching among these three states depends on both outside-in and inside-out allostery. The external ligand binding (ELB) pocket of I-domain-lacking integrins, serving as the starting point of outside-in allostery or the end point of inside-out allostery (10), is jointly formed by βI domain of β-subunit and β-propeller domain of α-subunit. ELB activates βI domain, and hence, the Hybrid domain swings out $\sim$70 Å. The Hybrid domain swing weakens the interactions between

the headpiece and tailpiece and also between α- and β-subunits to induce integrin stand-up and two-leg separation, leading to outside-in signaling. For inside-out signaling, the allostery flows along the reversed direction. Specifically, the allosteric pathway of the I-domain-containing integrins is very complicated because the existence of αI domain introduces additional conformational transmission between αI and βI domains. As a connecting link, αI domain not only serves as the binding pocket of external ligand by its metal ion-dependent adhesion site (MIDAS) but also binds to the pocket of βI domain as an internal ligand (12–14). The allosteric features of αI domain itself are quite clear and involved in MIDAS relocation and α_7-helix downward movement (15,16). As typical αI-domain-present integrins, original x-ray crystallographic structures of β_2 integrin with full ectodomains or headpieces also offer insights in understanding the global conformational features of different states (17–19). However, the linkage between α- and β-subunits and, in particular, the allosteric dynamics at microstructural level, remain unclear. For instance, the respective roles of ELB or internal

ligand binding (ILB) as well as their cooperation are ambiguous even though the ligand binding is known to activate outside-in signaling.

αI-domain α_7-helix-downward movement facilitates the capture by βI domain pocket and transmits the conformational change from α- to β-subunits (5,20). Similar downward displacement of βI domain α_7-helix causes the swinging out of Hybrid domain (21,22), which extends to the knee, translocates the lower legs of β-subunit laterally, and exerts forces on cytoskeleton by β-subunit cytoplasmic domain that binding to talin or kindlin (10,23,24). High-resolution x-ray crystallographic structures elaborate their conformations. As to the intrasubunit conformational transmission between βI and Hybrid domains of the β-subunit, $\alpha_{IIb}\beta_3$ structures show that Hybrid domain swings out $\sim$70 Å with fully activated βI domain (10,22,25), whereas the structures of β_2 and β_3 integrins indicate that βI domain activation does not necessarily cause the Hybrid domain swingout (18,26). Furthermore, the swingout of the Hybrid domain appears with the inactivated βI domain (27). In addition, structural details of βI domain conformation are lacked when visualizing fully swingout of the Hybrid domain with electron microscopy (EM) (8,28,29). Evidently, the correlation between the Hybrid domain movement and βI domain conformation is unclear.

Using typical crystal structures of $\alpha_X\beta_2$ integrin (17,18), molecular dynamics (MD) simulations were employed here to investigate the first two steps of outside-in activation of I-domain-containing integrin, including respective contributions of ELB and ILB to conformational allostery and transmission as well as their cooperative effects. Allosteric pathways were then discussed, which provided a, to our knowledge, new insight into understanding the allosteric dynamics of I-domain-containing integrin.

MATERIALS AND METHODS

System setup

Four head domains, including αI and β-propeller domains of α-subunit (residue 1–597) and βI and Hybrid domains of β-subunit (residues 59–423), were extracted from complete ectodomain crystal structures of the $\alpha_X\beta_2$ integrin (Protein Data Bank (PDB) codes of PDB: 3K6S (17), PDB: 4NEH, and PDB: 4NEN (18)) for simulations. These four domains are necessary and sufficient to study the first two steps of outside-in activation of the I-domain-containing integrin. That is, the αI and βI domains are key in conformational transmission; the β-propeller domain is required to stabilize βI domain conformation, and the Hybrid domain is the indicator of outside-in signaling. For building up the $\alpha_X\beta_2$-ICAM-1 complex, the crystal structure of ICAM-1 D3 domain (PDB: 2OZ4, residue 186–284 (30)) was separated and docked to I domain, as described before (31). Briefly, using VMD (32) Plugin MultiSeq (33) software, the α_X I domain and ICAM-1 D3 domain were respectively aligned to their similar complex of the IA LFA-1 I domain-ICAM-1 D1 complex for defining the proper initial positions (Fig. 1 A; (5)). Then, a 200-pN external force was applied on the side-chain oxygen of D229 of ICAM-1 D3 domain with constantly adjusted direction from the pulled oxygen atom to the fixed MIDAS ion of α_X I domain until it had bound to the ion (Fig. 1

B, upper right insert). This force-induced binding procedure is a compromising strategy to accelerate ELB within acceptable simulation time. To a certain extent, this force-induced ligand binding strategy is also physiologically reasonable by mimicking the receptor ligand binding resulted from colliding of flowing leukocytes to endothelial cells in blood flow. Similar force-induced binding procedure was also applied to ILB by applying the force on one side-chain oxygen of E318 residue of α_X I domain until it had bound to the MIDAS ion of the β_2-I-like domain (Fig. 1 B, lower right insert). Also, D229 of external ligand ICAM-1 or E318 of αI domain was assumed to bind to MIDAS(I) or MIDAS(I-like) ion if the pulled side-chain oxygen atom was close to respective metal ions by 3.5 Å. It should be noted that the missed ions in the synergistic metal ion-binding site (SYMBS) and MIDAS sites of βI domain of crystal structure 3K6S were added using the similar docking method as described above. In brief, this procedure was based on the preconditions of high homology between βI domain of β_2 and β_3 integrins as well as the presence of all SYMBS, MIDAS, and adjacent to MIDAS (ADMIDAS) ions in one crystal structure of $\alpha_{IIb}\beta_3$ integrin (PDB: 3FCS). βI domain of 3K6S was superposed to that of 3FCS, and the SYMBS and MIDAS ions of 3FCS were adopted to 3K6S for defining the initial positions of the two absent ions. The locations of these two ions were optimized by subsequent energy minimization and free equilibration.

MD simulations

Each simulation system was built up by solvating the target molecule(s) into a rectangular water box and neutralized with $\sim$100 mM Na^+ and Cl^- ions (Fig. 1 B, left). The system of four head domains contains $\sim$203,000 atoms, and the one with external ligand of ICAM-1 D3 domain contains $\sim$257,000 atoms. NAMD program (34) with CHARMM27 all-atom force field (35) was used. An integration time step of 1 fs and the periodic boundary conditions were applied in the simulations. A smooth (10–12-Å) cutoff and the particle mesh Ewald method were employed to calculate van der Waals forces and full electrostatics, respectively. A 300-K heat bath was manipulated under Langevin thermostat, and 1 atm pressure was controlled by the Nosé-Hoover Langevin piston method. Before the equilibration process, energy minimization was performed with 10,000 steps of fixed backbone atoms followed by an additional 10,000 steps with all atoms free for the system heated from 0 to 300 K at 30-K increments every 5 ps. A 10-ns or longer equilibration was performed for each system.

Steered MD (SMD) simulations were also conducted to accelerate the allostery or unbind the $\alpha_X\beta_2$-ICAM-1 complex (36). Complex conformations resulted from above equilibrations served as the initial conformation for corresponding SMD simulations. Here, C-terminal C_α atom of Hybrid domain was fixed, and a constant force of 10, 20, 50,100, 200, 400, or 800 pN was applied on C-terminal C_α atom of ICAM-1 D3 along the vector from the fixed atom to the pulled end (Fig. 1 B, left). Lifetime of the complex was defined from SMD simulations as the time interval required to separate the MIDAS ion away from the side-chain oxygen of D229 of ICAM-1 D3 domain or E318 of I domain around 10 Å.

Simulation designs

Simulation design was described in Fig. 1 C. The head domains from crystal structure 3K6S with closed αI and βI domains and unbound internal ligand was depicted as Fig. 1 Ca, and those from crystal structure 4NEH-4NEN with open αI domain, and bound internal ligand was depicted as Fig. 1 Cd. Three simulation sets were designed for investigating the conformational allostery of $\alpha_x\beta_2$ head domains using different binding orders of external or ILBs. The first set was abbreviated as $\overrightarrow{EIF}$, which represented the sequential simulations from ELB through ILB to force-induced allostery or dissociation (FAD), $C_a \rightarrow C_b \rightarrow C_e \rightarrow C_g \rightarrow C_h$. The second was abbreviated as $\overrightarrow{IEF}$ with the reverse order, $C_a \rightarrow C_c \rightarrow C_f \rightarrow C_g \rightarrow C_h$. And the last one was abbreviated as $\overrightarrow{EF}$, which only included ELB and FAD

based on the internal ligand-bound structure of 4NEH-4NEN, $C_d \rightarrow C_f \rightarrow C_g \rightarrow C_h$ (Fig. 1 C).

Free MD simulations were also conducted to evaluate the conformational stability at each stage, including external ligand absence (w/o EL), after ELB (equilibrated (Eq)-ELB), after ILB (Eq-ILB), and after FAD (Eq-FAD). The last frame of ELB, ILB, or FAD simulation was set as respective starting one for after free MD simulations right after the removal of external force. All the simulations were summarized in Table 1. In total, 2090-ns equilibration MD simulations and 1465.6-ns SMD simulations were performed in this work.

Simulation analyses

Firstly, different geometry parameters were defined to represent the conformational characteristics of $\alpha_X\beta_2$ integrin using the coordinate of the key residue or the relative angle of typical vector. The stable core residues of βI domain were aligned among crystal structures of the $\alpha_X\beta_2$ integrin 3K6S and 4NEH and one of the $\alpha_{IIb}\beta_3$ integrin (PDB: 2VDL). The corresponding coordinates of MIDAS(I) ion in the 3K6S and 4NEH α-subunits were respectively represented as the closed and open states of I domain, and those of the atomic center of P59-C_α and C423-C_α in 3K6S and 2VDL β-subunits were respectively denoted as the closed and swingout of the Hybrid domain. The coordinates of MIDAS(I) and atomic center of P59-C_α and C423-C_α of trajectory snapshots, after the same alignment of their βI domain to that of 3K6S, were used to describe the conformational evolution during simulations. The orientation of αI and Hybrid domains were also quantified between different reference structures or between simulation snapshot and reference structure. This was defined by the relative angle of the vector from E130-C_α atom to MIDAS(I) ion of the αI domain or the vector from the center of K101-C_α and S343-C_α atoms to the center of P59-C_α and C423-C_α atoms of Hybrid domain. The angle for αI domain swinging from the inactivated state of 3K6S to the activated state of 4NEH was $\sim58°$, and the one for Hybrid domain swinging when activated was $\sim68°$ (Fig. 2 A). In addition, based on the respective alignments of the stable core residues

of the αI or βI domain trajectory conformations to that of crystal structure with LA or HA conformation, the root mean-square deviation (RMSD) of the αI or βI domain α_7-helix was calculated to investigate the conformational features of the trajectory snapshots. VMD program was used for data analysis and conformation presentation (32).

RESULTS

Different binding orders of external and internal ligands induced distinct conformational transmission

Orientation variations of both αI and Hybrid domains are the most significant allosteric features of integrin headpieces. Superposing crystal structures $\alpha_X\beta_2$ integrin 3K6S and 4NEH with $\alpha_{IIb}\beta_3$ integrin 2VDL, the αI domain swingout was estimated to be $\sim58°$ along anticlockwise direction from the closed state (3K6S) to the open state (4NEH) and the Hybrid domain swingout $\sim68°$ from its closed state (3K6S) to corresponding open state (2VDL) (Fig. 2 A).

To characterize the conformational features and corresponding dynamic evolutions of $\alpha_X\beta_2$ integrin, the coordinate of αI domain MIDAS(I) ion (*black diamond* and *green squares*) and the centers of Hybrid domain P59-C_α and C423-C_α atoms (*green triangle* and *black star*) from both open and closed crystal structures were shown as references based on the alignment of βI domain backbone atoms (Fig. 2 B). The results from two typical runs of 100-ns free-equilibration simulations without either ELB or ILB showed that the closed $\alpha_X\beta_2$ headpieces retained its LA state with slight fluctuations of both αI (*red* and *cyan dots*) and Hybrid

TABLE 1 Summary of MD Simulations

		Simulations (Duration (ns) × Runs)												
		Free MD			Force-Induced Binding (200 pN)		Force-Induced Allostery/Dissociation							
System	PDB Code	w/o EL	Eq-ELB	Eq-ILB	Eq-FAD	ELB	ILB	10 pN	20 pN	50 pN	100 pN	200 pN	400 pN	800 pN
ELB→ILB→ FAD ($\overrightarrow{EIF}$)	3K6S; 2OZ4	–	100 × 2	100 × 3	10 × 1 100 × 1	20 × 1 25 × 2 35 × 1 38 × 1 50 × 1	30 × 1 35 × 2 40 × 1	16 × 1 20 × 1	16 × 1 20 × 1	16 × 1 20 × 1	10 × 1 16 × 1	5 × 1 6 × 1	10 × 3 2.5 × 3	1 × 1 3 × 4 3.1 × 1 1 × 3
ILB→ELB→ FAD ($\overrightarrow{IEF}$)	3K6S; 2OZ4	10 × 1 100 × 2	100 × 2	100 × 2	100 × 1	12 × 1 14 × 1 15 × 1 16 × 1	50 × 1 55 × 1 65 × 1	40 × 1	40 × 1	30 × 1	30 × 1	20 × 1	10 × 3	7 × 1 9 × 1 10 × 1 23 × 1
ELB→FAD ($\overrightarrow{EF}$)	4NEH/4N4N; 2OZ4	10 × 7 100 × 3	100 × 1	100 × 1	100 × 2	2 × 1 6 × 1 8 × 1 9 × 1 14 × 2 24 × 1 29 × 1 39 × 1	24 × 1 34 × 1 39 × 1 46 × 1 50 × 2 60 × 1 – –	–	–	–	4 × 1	–	–	1 × 3 2 × 2 20 × 1

PDB codes PDB: 3K6S, PDB: 4NEH, and PDB: 4NEN are given for $\alpha_X\beta_2$ and PDB: 2OZ4 for ICAM-1. ELB, external ligand binding; Eq, equilibrium; FAD, force-induced allostery or dissociation; ILB, internal ligand binding; w/o EL, without external ligand presenting.
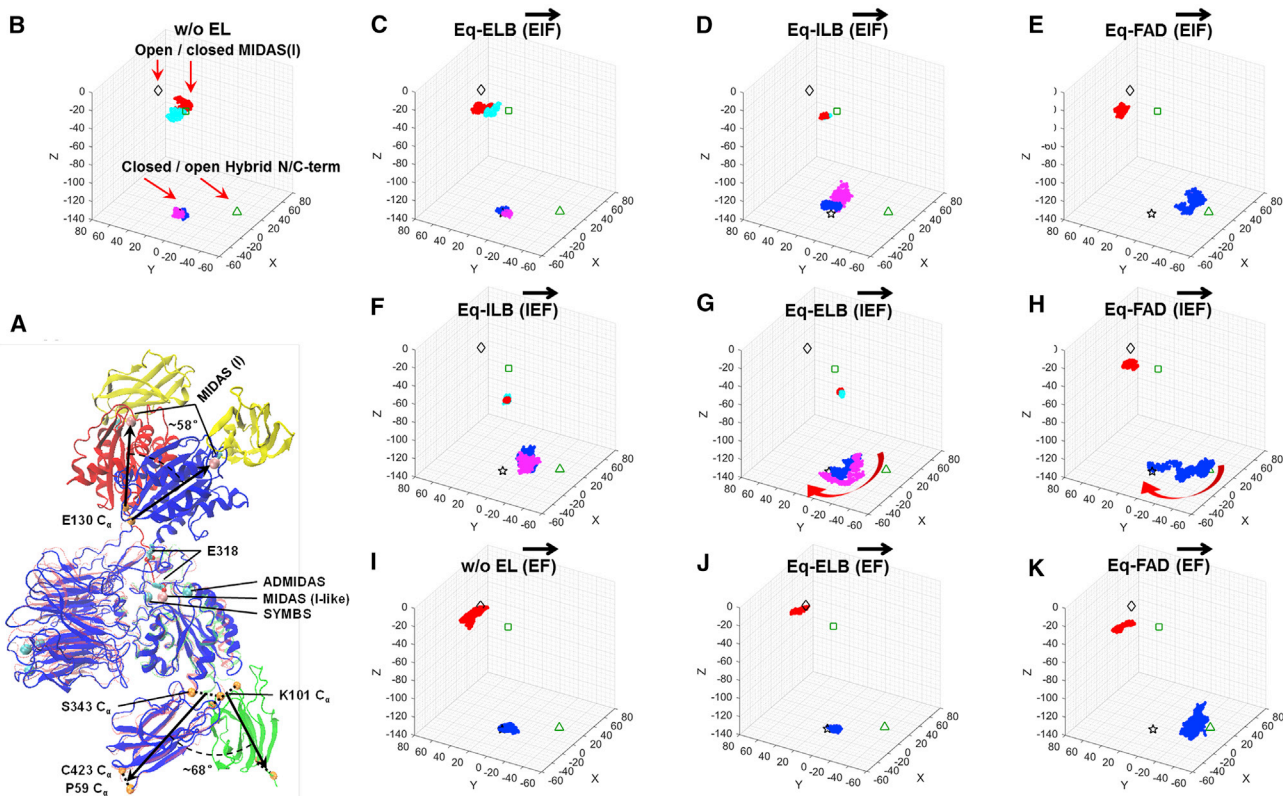
FIGURE 2 Orientation evolutions of I and Hybrid domains during free equilibrations of different stages. (*A*) Structural superposition for the crystal structures of $\alpha_X\beta_2$ integrin 3K6S (*blue*) and 4NEH (*red*) and $\alpha_{IIb}\beta_3$ integrin 2VDL (*green*) based on the backbone atom alignment of the I-like domain. The external ligand of ICAM-1 (*yellow*) was also shown. The orientation of I domain was defined by vector from C_α atom of E130 to MIDAS(I) ion, and the angle of I domain swinging from inactivated to activated states was ~58°. The orientation of the Hybrid domain was defined by the vector from center of C_α atoms of K101 and S343 to center of C_α atoms of P59 and C423, and the angle of the Hybrid domain swinging when activated is ~68°. C_α atoms of E130, K101, S343, P59, and C423 were presented in orange VDW, MIDAS(I), MIDAS(I-like), ADMIDAS, and SYMBS ions were shown in purple or cyan VDW, and the internal ligand of E318 was shown in name licorice. (*B*) Coordinates of MIDAS(I) ion were shown to illustrate the orientations of the αI domain of different conformational states with a black diamond for open state, a green square for close state, and red and cyan dots for equilibration simulations. The center of C_α atoms of P59 and C423 were shown to illustrate those of Hybrid domains with a green triangle for open state, black star for close state, and blue and purple dots for equilibration simulations. (*B–K*) Orientation evolutions of I and Hybrid domains during free equilibrations were presented in (*B*)–(*K*). The panels in the cases of w/o EL (*B*), Eq-ELB ($\overrightarrow{EIF}$) (*C*), Eq-ILB ($\overrightarrow{EIF}$) (*D*), and Eq-FAD ($\overrightarrow{EIF}$) (*E*) denoted the equilibrated (Eq) states for sequential $\overrightarrow{EIF}$ simulations of crystal structure 3K6S after forced ELB, ILB, and FAD, respectively. The ones of (*B*) and (*F*)–(*H*) and (*I*)–(*K*) were for corresponding $\overrightarrow{IEF}$ and $\overrightarrow{EF}$ orders, respectively. Each equilibration simulation was performed for 100 ns, and the orientations were extracted from trajectory snapshots every 0.2 ns. Different colors in the panels represented different equilibration repeats. Those of crystal structures were presented in each panel for reference. The arrows in (*G*)–(*H*) indicated the orientation evolutions along the equilibration time. To see this figure in color, go online.

(*blue* and *purple dots*) domains around their initial states (Fig. 2 *B*). The initial ELB induced the deviation of αI domain from its initial state and the intactness of Hybrid domain (Fig. 2 *C*). However, the Hybrid domain became flexible with higher fluctuation after the followed ILB even though the αI domain returned back to its initial orientation, indicating that the allosteric signals are transmitted from α-subunit to β-subunit (Fig. 2 *D*). After FAD, both αI and Hybrid domains retained their open states stably, and the αI domain even surpassed the position of open crystal structure (Fig. 2 *E*; Video S1). Collectively, $\alpha_X\beta_2$ integrin during $\overrightarrow{EIF}$ processes experiences conformational transmission from the α-subunit to β-subunit and realizes the allostery of both αI and Hybrid domains from corresponding closed state to open state (Fig. 2, *C–E*). In contrast, distinct

behaviors were demonstrated during $\overrightarrow{IEF}$ processes (Fig. 2, *F–H*). Although the conformational transmission from the α-subunit to β-subunit was achieved by the first ILB with the deviation of Hybrid domain from its initial closed orientation (Fig. 2 *F*), it returned back to its closed state after ELB (Figs. 2 *G* and S1, *A–C*; Video S2) and further FAD simulations even with the opening of αI domain (Figs. 2 *H* and S1, *A* and *D*; Video S3). Reversible dynamics of Hybrid domain were shown in Fig. S1, *B–D*, with red or black lines indicating the angles between equilibration conformations and closed or open crystal structure. Interestingly, a new orientation (*green*) of Hybrid domain distinct from both the closed (*black*) and open (*purple*) states was presented right after ELB, with the feature of pointing out from the plane (Fig. S1 *A*). This orientation was not stable

and tended to rotate back to the closed state (*red*) after the following free-equilibration simulations (Fig. S1, *A–C*). Similar behaviors were presented in FAD simulations, in which the semiopen conformation (*blue*) was induced right after FAD but returned to the closed state during the following free-equilibration simulations (Fig. S1 *D*). These results indicated that Hybrid domain prefers to retain closed state during $\overrightarrow{IEF}$ processes, suggesting that the signals from outside are blocked if internal ligand binds first. It was also demonstrated that ILB is necessary for Hybrid domain allostery based on the conformational changes of Hybrid domain before and after ILB in both $\overrightarrow{EIF}$ and $\overrightarrow{IEF}$ sets (Fig. 2, *D* and *F*).

As a reference, simulations were also performed using the $\alpha_X\beta_2$ crystal structure of 4NEH with the open state of the αI domain and bound internal ligand (Fig. 2, *I–K*). The results demonstrated that αI and Hybrid domains retained their respective open and closed conformations during free-equilibration simulations in the case of both w/o EL (Fig. 2 *I*) and after ELB (Fig. 2 *J*). The Hybrid domain swung to open state under unbinding force and stayed stable during the following free MD simulation, whereas αI domain surpassed the open state again as it did during $\overrightarrow{EIF}$ or $\overrightarrow{IEF}$ processes (Fig. 2 *K*; Video S4). The simulations also indicated that the, to our knowledge, novel position of αI domain might be its real open state after FAD. It is hard to tell if the $\overrightarrow{EF}$ set is similar to $\overrightarrow{EIF}$ or $\overrightarrow{IEF}$ set because of the existing open αI domain and bound internal ligand of crystal structure 4NEH. It seemed contradictory with those of $\overrightarrow{EIF}$ or $\overrightarrow{IEF}$ that the Hybrid domain stayed in closed state stably with ILB before applying unbinding force. Nevertheless, dynamic evolutions of αI and Hybrid domains during corresponding SMD simulations were also shown in Fig. S2. All snapshots of repeated SMD simulation trajectories were pooled together. In combination of SMD simulations for $\overrightarrow{EIF}$ (Fig. S2, *A–C*), $\overrightarrow{IEF}$ (Fig. S2, *D–F*), and $\overrightarrow{EF}$ (Fig. S2, *G–H*) sets with corresponding free-equilibration simulations (Fig. 2, *B–K*), the results indicated that 1) ILB is required for allosteric transmission from the α-subunit to β-subunit, and 2) a different binding order for ELB and ILB induces distinct signaling.

Different binding orders of external and internal ligands induced distinct allostery of αI and βI domains

The conformational transmission along intersubunits or intrasubunits depends on the allostery of αI and βI domains. To quantify allosteric features of αI and βI domains and elucidate the relevance between their allosteric pathway and conformational transmission, the RMSD of αI or βI domain α_7-helix relative to their respective closed state was calculated based on the backbone atom alignment of αI or βI domain to the closed structure 3K6S. The probability distributions of RMSD showed that the αI domain re-

tained the closed state during initial free-equilibration simulations in w/o EL case, followed by step-by-step activation based on sequential ELB (ILB), ILB (ELB), and FAD processes in both $\overrightarrow{EIF}$ (Fig. 3 *A*) and $\overrightarrow{IEF}$ (Fig. 3 *C*) sets. Corresponding conformations of respective simulation end point demonstrated that αI domain α_7-helix moved downward along the helix axis in both $\overrightarrow{EIF}$ and $\overrightarrow{IEF}$ sets with respective manners. During $\overrightarrow{EIF}$ simulations, the residue of F300 rotated out of the hydrophobic pocket gradually from w/o EL (*black*), Eq-ELB (*red*), Eq-ILB (*green*), to Eq-FAD (*blue*) simulations and then moved downward, and the residue E318 showed similar behaviors with gradual deviation from its initial position and unfolding of upriver helix (Fig. 3 *A′*). During $\overrightarrow{IEF}$ simulations, the residue F300 moved downward directly without rotation from its hydrophobic pocket, and E318 stayed still in its initial position until it was pulled in FAD simulation (Fig. 3 *C′*). The RMSDs of the αI domain in $\overrightarrow{EF}$ simulations showed similar distributions among w/o EL, eq-ELB, and eq-FAD (Fig. 3 *E*), also comparable with those of Eq-FAD simulations in both $\overrightarrow{EIF}$ and $\overrightarrow{IEF}$ sets (Fig. 3, *A* and *C*, *blue*). This is reasonable because the αI domain in 4NEH structure is already in open state in $\overrightarrow{EF}$ set. Corresponding end-point snapshots showed similar features with those of $\overrightarrow{EIF}$ set, including the deviation of F300 from hydrophobic pocket, the downward movements of both F300 and E318, and the unfolding of upriver helix of E318 (Fig. 3 *E′*). Moreover, the conformational evolutions of the αI domain in different sets were also represented using αI domain α_7-helix RMSD of snapshots to the reference conformation of open state. The results showed the consistency with those of RMSDs to the reference conformation of closed state. The RMSD distributions gradually shifted left, after the sequential stages in both $\overrightarrow{EIF}$ (Fig. S3 *A*) and $\overrightarrow{IEF}$ (Fig. S3 *B*) sets and always retained low values in $\overrightarrow{EF}$ set (Fig. S3 *C*).

The RMSD distributions of βI domain α_7-helix and corresponding conformations were shown in Fig. 3 *B*, *D*, *F*, *B′*, *D′*, and *F′*, respectively. The results demonstrated that the βI domain was activated gradually with right-shifted RMSD distributions in $\overrightarrow{EIF}$ set (Fig. 3 *B*). Corresponding end-point snapshots showed similar features with those of the αI domain, where the side chain of V330 rotated clockwise and moved down along the helix axis (Fig. 3 *B′*). In $\overrightarrow{IEF}$ set, the first two stages of ILB and ELB did not induce obvious changes of the βI domain with comparable RMSD distributions with those of w/o EL equilibration simulations (Fig. 3 *D*). Although the RMSD distribution at the last stage of Eq-FAD shifted right, it did not represent the actual allostery because the βI domain α_7-helix did not have obvious downward movement except of terminal unfolding of the α_7-helix (Fig. 3, *D* and *D′*). In the $\overrightarrow{EF}$ set, the RMSD distribution shifted slightly right after the last stage of FAD simulations (Fig. 3 *F*). Even not obvious as that at the last stage of $\overrightarrow{EIF}$ set, the βI domain α_7-helix tended to move downward along the helix axis (Fig. 3 *F'*).

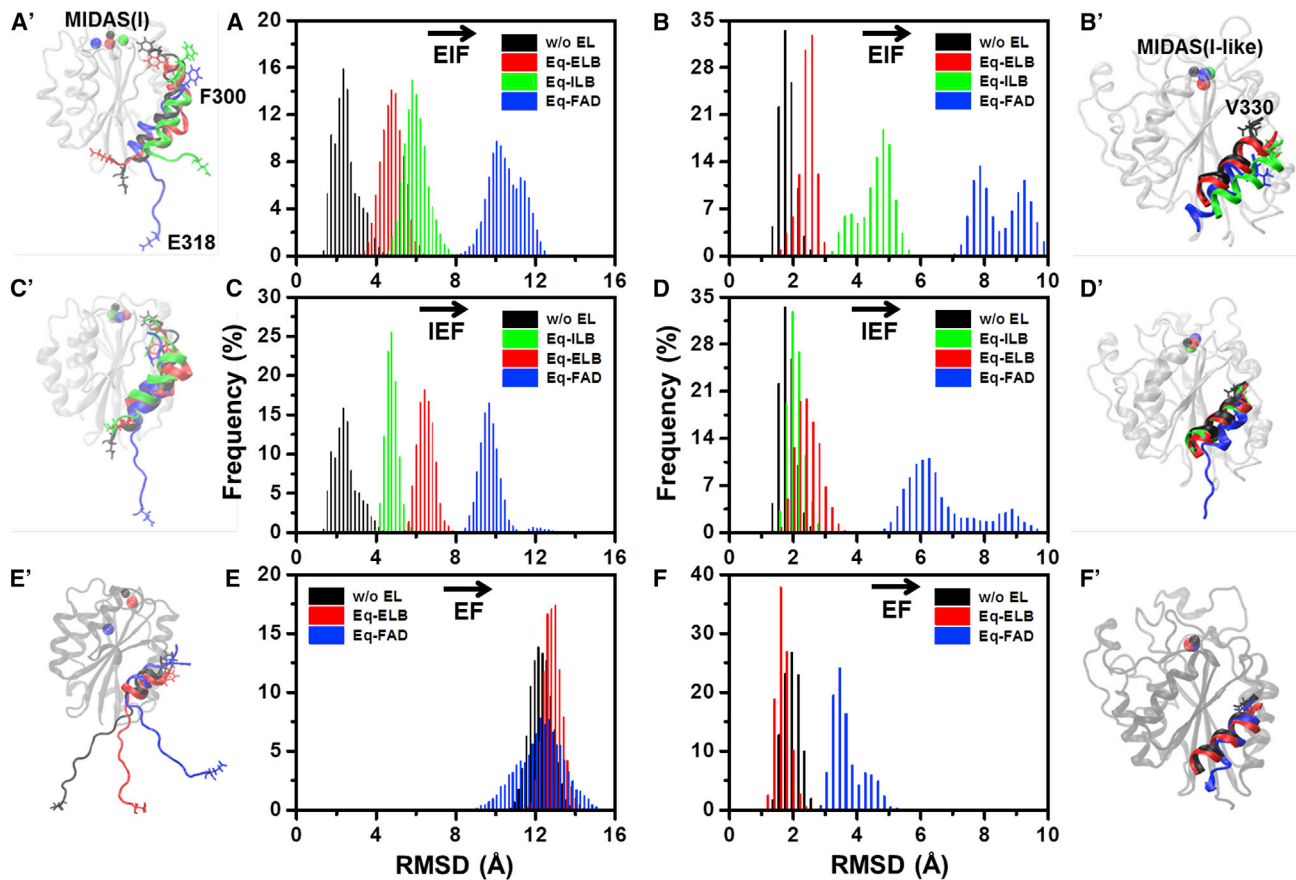FIGURE 3 Allostery of I and I-like domains during free equilibrations of different stages. (A–F) The probability distributions of RMSD for α_7-helixes in both I (A, C, and E) and I-like (B, D, and F) domains were presented in (A) and (B) for $\overrightarrow{EIF}$, (C) and (D) for $\overrightarrow{IEF}$, and (E) and (F) for $\overrightarrow{EF}$ orders, respectively. The corresponding conformation comparisons were shown in (A')–(F'), with structural superposition of final equilibration snapshots of different stages. The RMSDs were calculated based on the backbone atom alignment of I- or I-like-domain-center β-sheets of simulation snapshots to those of crystal structure 3K6S. The binned data (A–F) or conformations (A'–F') for equilibrations in the cases of w/o EL, Eq-ELB, Eq-ILB, and Eq-FAD were presented in black, red, green, and blue, respectively. Only α_7-helixes of the I or I-like domain were highlighted in opaque newcartoon in (A')–(F'). To see this figure in color, go online.

It should be noted that the difficulties of the forced complex dissociation and the Hybrid allostery at FAD stage were different among $\overrightarrow{EIF}$, $\overrightarrow{IEF}$, and $\overrightarrow{EF}$ sets. It was easiest in $\overrightarrow{EIF}$ set but most difficult in the $\overrightarrow{EF}$ set, as seen in the results that the force applied for FAD simulations gradually increased from $\overrightarrow{EIF}$ then $\overrightarrow{IEF}$ to $\overrightarrow{EF}$ sets (Table 1). In fact, the applied force was 100 pN for $\overrightarrow{EIF}$ (Fig. S2 C), 200 pN for $\overrightarrow{IEF}$ (Fig. S2 F), and 800 pN for $\overrightarrow{EF}$ (Fig. S2 H) sets. The slight allostery of βI domain α_7-helix in the $\overrightarrow{EF}$ set may be relevant with these difficulties at FAD stage.

In brief, combining dynamic trajectory evolutions (Fig. 2) with RMSD distributions and conformational characteristics of the βI domain (Fig. 3) indicated that the stable swingout of Hybrid domain depends on the activation of βI domain and that the inactivation state of the βI domain contributes to the rotating back of the Hybrid domain in the $\overrightarrow{IEF}$ set. Furthermore, elaborative conformational differences of the αI domain among three sets implied that not only α_7-helix downward movement followed αI domain activation, but

the rotation out of F300 from the hydrophobic core and E318 extending with its upriver helix unfolding also play a role in effective conformational transmission from α-subunit to β-subunit.

Allostery of the αI domain regulated the force-induced receptor ligand binding

In fact, the allostery of the αI domain not only regulates the orientation of both αI and Hybrid domains but also affects the ability of ligand binding. The mean association time for both ELB and ILB were calculated from different sets. Results showed that the ELB became easier with shorter time in the sets of $\overrightarrow{IEF}$ (second bar) and $\overrightarrow{EF}$ (third bar) than that of $\overrightarrow{EIF}$ (first bar) (Fig. 4), implying that the allostery of the αI domain induced by ILB in both $\overrightarrow{IEF}$ and $\overrightarrow{EF}$ sets could promote ELB. This seemed reasonable because α_7-helix downward movement would induce the exposure of ELB sites, even though there was no actual
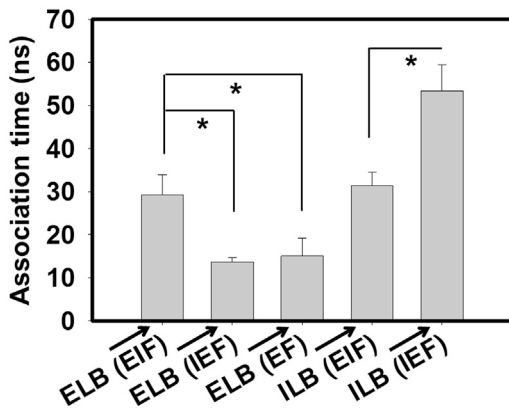
FIGURE 4 Association time differences of force-induced receptor ligand binding among $\overrightarrow{EIF}$, $\overrightarrow{IEF}$, and $\overrightarrow{EF}$ simulations. The times for forced ELB were compared among $\overrightarrow{EIF}$, $\overrightarrow{IEF}$, and $\overrightarrow{EF}$ orders (*left three bars*) and for forced ILB between $\overrightarrow{EIF}$ and $\overrightarrow{IEF}$ orders (*right two bars*). At least three runs of simulations were repeated for each case. *$p < 0.05$.

allostery of αI domain in $\overrightarrow{IEF}$ set. The association time for ILB was also compared between the $\overrightarrow{EIF}$ and $\overrightarrow{IEF}$ sets, with significantly shorter time in $\overrightarrow{EIF}$ set (*fourth bar*) than that in the $\overrightarrow{IEF}$ set (*fifth bar*) (Fig. 4). The first stage of ELB in $\overrightarrow{EIF}$ had already activated the αI domain partially and induced E318 extending, and the enhanced freedom of internal ligand E318 would speed its binding to the βI domain. Collectively, the conformational change of αI domain α_7-helix plays a pivot role by bridging the ELB epitope of the αI domain and ILB.

Unfolding of α_7-helix during αI domain allostery facilitated intersubunit conformational transmission

The above results indicated that αI domain allostery affects both ELB and ILB. In addition to the featured downward movement of entire α_7-helix, most simulations showed the unfolding of its lower half helix during αI domain allostery. Here, we further analyzed the conformational changes of this partial unfolding to decipher the underlying biological relevance and function. First compared were the conformations of α_7-helix in closed (Fig. 5 A) and open (Fig. 5 H) states. In addition to the downward movement of entire α_7-helix, its internal conformation was also changed significantly after activation. The key feature lied in the unfolding of the lower half helix (Q307-A316) with the intact upper half (D301-I306). Integrating dynamic conformational evolutions in both $\overrightarrow{EIF}$ and $\overrightarrow{IEF}$ sets, the possible allosteric pathway of αI domain α_7-helix from the closed to the open state was outlined. The conformational evolutions in $\overrightarrow{EIF}$ set indicated that the α_7-helix moved downward slightly with intact helix conformation right after ELB, providing an additional space for the swinging of internal ligand of E318 and C-linker and then facilitating ILB (Figs. 3, A and A' and 5 B; colored in *red*). The followed ILB induced the flipping

out of the F300 side chain from the hydrophobic core, and the α_7-helix further moved downward as a whole. During this stage, the orientations of the lower half helix and C-linker were also adjusted and ready for further allostery (Figs. 3, A and A' and 5 C; colored in *green*). After the last FAD stage, the conformation of α_7-helix became very similar to the open state with the unfolding of the lower-half helix (Figs. 3, A and A' and 5 D; colored in *blue*). These analyses indicated that the lower-half α_7-helix unfolding has two functions. On the one hand, it offsets the 20-Å distance between internal ligand of E318 and MIDAS(I-like) ion in closed state for ILB. On the other hand, it also guarantees the distance requirement for both αI domain reorientation and ILB.

By contrast, the conformational evolutions in $\overrightarrow{IEF}$ set showed distinct features. The first stage of ILB was compulsory with the closed state of α_7-helix, which induced minor passive downward movement of the α_7-helix by retaining the F300 side chain in the hydrophobic core (Figs. 3, B and B' and 5 B; colored in *green*). Thus, the 20-Å distance between E318 and MIDAS(I-like) ion was achieved only by the orientation change of αI domain. The followed ELB (Figs. 3, B and B' and 5 F; colored in *red*) and FAD (Figs. 3, B and B' and 5 G; colored in *blue*) stages gradually induced the α_7-helix to the semiopen state. In fact, the F300 side chain always inserted in the hydrophobic core, hindering the smooth downward movement of entire α_7-helix and resulting in the structural disruption of the helix (Fig. 5 G). Taken together, the $\overrightarrow{EIF}$ set presents reasonable pathway for forced outside-in activation of $\alpha_X\beta_2$ integrin but $\overrightarrow{IEF}$ set does not. Unfolding of the lower-half α_7-helix of the αI domain could be biologically relevant for effective ILB and conformational transmission.

DISCUSSION

Studies in structural and computational biology have greatly enhanced the understandings of how the allostery of I-domain-absent integrins work (21,37–39), but the knowledge for those I-domain-containing integrins is relatively limited. Existing crystal structures only present two isolated states of the $\alpha_X\beta_2$ integrin and headpieces of $\alpha_L\beta_2$, all of which are bent with closed headpieces (17–19). EM studies demonstrate static and blurry configurations of Hybrid domain opening in which the details of αI and βI domain conformations are missing (40). As to the two key steps for outside-in activation of I-domain-containing integrins, the preferred orders for ELB and ILB remain unclear because of the limitations of experimental techniques. With the specific designs with inverse binding orders of external and internal ligands, this work investigated the conformational evolution features of the $\alpha_X\beta_2$ headpiece domains in closed state using MD simulations. The results showed entirely different behaviors by reverse binding orders of external and internal ligands. When the external
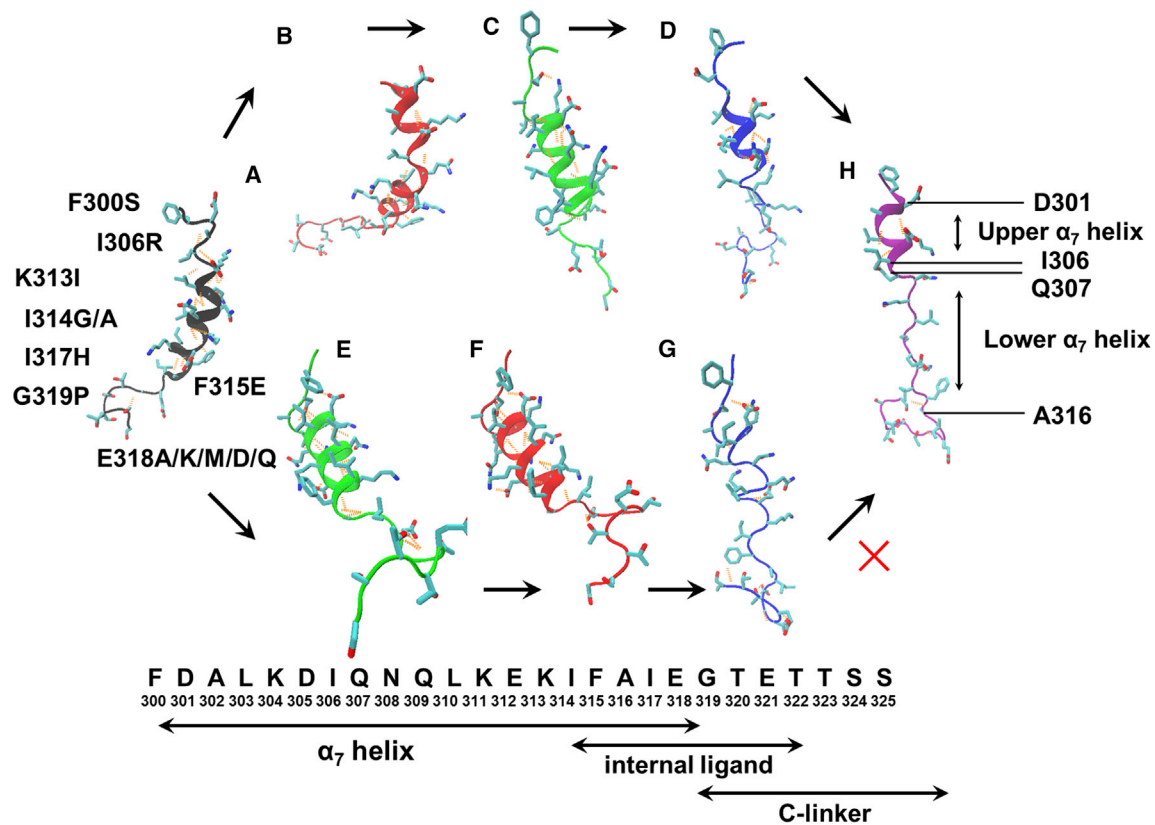
FIGURE 5 Unfolding distinction of I domain α_7-helix between $\overrightarrow{\text{EIF}}$ and $\overrightarrow{\text{IEF}}$ simulations. The crystal structures of I domain α_7-helix and C-linker of closed (3K6S) and open (4NEH) states were demonstrated in (A) and (H), respectively. The typical conformations of three equilibration stages of $\overrightarrow{\text{EIF}}$ and $\overrightarrow{\text{IEF}}$ sets were shown in (B)–(D) and (E)–(G), respectively. The amino acid sequences of I domain α_7-helix, internal ligand, and C-linker were shown at the bottom. The mutated sites from literature (18,42) were also indicated in (A). The red cross between (G) and (H) denoted the distinct conformations of I domain α_7-helix between the equilibration snapshot after FAD stage of $\overrightarrow{\text{IEF}}$ set and the open state of crystal structure 4NEH. To see this figure in color, go online.

ligand binds first to the αI domain, the α_7-helix moves downward with the exposure of internal ligand E318, and the αI domain orientation becomes more flexible (Figs. 2 A and 3 A), contributing cooperatively to ILB. Furthermore, αI domain F300 tends to flip out from the hydrophobic core, which facilitates the subsequent downward movement of α_7-helix. The secondary ILB then promotes an entire flipout of the αI domain F300 and furthers downward movement of α_7-helix. This stage also bridges the α-subunit αI domain and β-subunit βI domain and initiates the allostery of the βI domain with similar downward movement of its α_7-helix, which is transmitted to the Hybrid domain with slight swingout. Thus, the allostery and force transmission pathway remain unobstructed. Finally, the forced dissociation of integrin-external-ligand complex favors the complete allostery. A working model for this $\overrightarrow{\text{EIF}}$ process was then proposed in Fig. 6 A.

When the internal ligand binds first to the βI domain, the αI domain α_7-helix also moves downward slightly as that of ELB first. But the side chain of F300 is still locked in the hydrophobic core so that the αI domain is forced close to the βI domain, with the αI domain α_7-helix buried between

them. This compulsive binding does not induce obvious allostery of βI domain, but the deviation of the Hybrid domain takes place from its closed state. The secondary ELB further pushes αI domain α_7-helix down with no activation of the βI domain. These results show an interesting behavior that the Hybrid domain rotates to a new orientation perpendicular to both the closed and open states, which can rotate back to the closed state once the binding force is withdrawn. This feature confirms again that the allostery of the βI domain is necessary for stable conformational transmission from the βI domain to Hybrid domain. Again, a working model for this $\overrightarrow{\text{IEF}}$ process was proposed in Fig. 6 B. Because of the inactivation of βI domain, the force-induced semiopen state of the Hybrid domain during FAD stage is still unstable and also able to rotate back to the closed state after removing the force. In conclusion, locking the αI domain F300 side chain in the hydrophobic core hinders the actual allostery of αI domain α_7-helix, which blocks the signal transmission between α- and β-subunits as well as followed allosteries of the βI domain and the Hybrid domain. These simulations suggest that there might be two pathways of outside-in activation for I-domain-
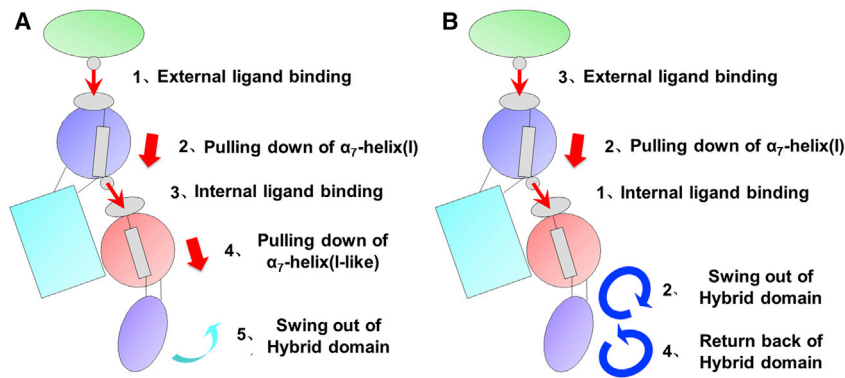
FIGURE 6 Schematic of two distinct allostery modes based on $\overrightarrow{EIF}$ and $\overrightarrow{IEF}$ orders. Typical allosteric features of I domain, I-like domain, and Hybrid domain for every stage of $\overrightarrow{EIF}$ and $\overrightarrow{IEF}$ orders were represented in (A) and (B), respectively. To see this figure in color, go online.

containing integrins, respectively starting from ELB or ILB, in a manner that the former facilitates allosteric transmission, and the latter impedes the transmission.

On the one hand, our simulations confirmed the reports in literature that ELB would activate $\alpha_x\beta_2$ αI domain, with rotating F300 out from the hydrophobic pocket and moving downward of α_7 helix, which is the same as the $\alpha_L\beta_2$ and $\alpha_M\beta_2$ αI domains do (31). They also supported that ILB is necessary for conformational transmission between α- and β-subunits and bearing external forces and that the allostery of the βI domain α_7-helix is precondition for stable swing-out of the Hybrid domain (13). These consistencies validated our simulations. Moreover, these all-atomic MD simulations in this work offered the visualized chain reactions of conformational transmission beyond static crystal structures, low-resolution EM profiles, or indirect experiments. To further testify the significance of ILB in bearing external forces, unbinding force was applied to the $\alpha_X\beta_2$-ICAM-1 complex when internal ligand was not bound (Table 1, second row in the FAD column of $\overrightarrow{EIF}$ set). It turned out that the nonbond interactions between the βI domain and β-propeller domain were not sufficiently strong, and α- and β-subunits dissociated very soon (e.g., 10 ns) under small external forces (e.g., 100 pN).

On the other hand, our simulations proposed a, to our knowledge, novel conformational state of the αI domain characterized by both the activation of the entire α_7-helix and its lower half unfolding around the internal ligand, as indicated for the internal-ligand-bound metastable state of $\alpha_X\beta_2$ from its crystalized structure (18). Setting the $\overrightarrow{EIF}$ and $\overrightarrow{EF}$ simulations that present partial unfolding of the αI domain α_7-helix could successfully realize stable swing-out of the Hybrid domain, but the $\overrightarrow{IEF}$ set without unraveling the unfolding of αI domain α_7-helix cannot possess the effective transmission. These results indicated that the unfolding of the internal-ligand-neighboring peptides of the αI domain is biologically relevant and plays a key role in conformational transmission from the α- to β-subunit. This is consistent with the fact that shorting the C-linker of the αI domain activates $\alpha_L\beta_2$ (41) because C-linker short-

ing results in the extension of α_7-helix. Meanwhile, various mutations of the αI domain α_7-helix in literatures also support the point (Fig. 5; (18,42)). Mutation of the αI domain I314G for destabilizing α_7-helix significantly increases the binding affinity of $\alpha_X\beta_2$ to iC3b, whereas the reverse mutation of F315E for stabling α_7-helix decreases the activation capability of $\alpha_X\beta_2$. Indeed, it is well known that the conformational transmission of integrins or other proteins depends on a complicated interaction network. In addition to the importance of α_7-helix, other pivotal sites are also reported to regulate the signal transmission of I-domain-containning integrins. For example, an upstream conserved Phe site in the αI domain α_1-helix acts as a pawl to stabilize the downward ratchet-like movement of the β_6-α_7 loop and α_7-helix (43). The downstream mutations of key residues around MIDAS of the βI domain decrease its binding to the conserved intrinsic ligand and followed activation of the αI domain (13). Also tested are the key roles of the αI domain MIDAS and βI domain MIDAS, SYMBS, and AD-MIDAS for allosteric transmission (44). Although this study mainly focuses on the contributions of α_7-helix to the intersubunit conformational transmission between the α- and β-subunits, further investigations are needed to explore global signaling pathway of the forced outside-in activation of I-domain-containing integrins.

In addition, the novel orientations of the αI domain and Hybrid domain, both of which rotates out plane, were first reported in this work to our knowledge. Various αI domain orientations presented in both $\alpha_L\beta_2$ and $\alpha_X\beta_2$ crystal structures suggest its surping flexibility (17–19). Applying ELB or external forces also possibly results in new orientations of the αI domain because of its long and remarkably flexible C-linker, which further enables the conformational relay via the integrin by exerting the tensile force to stabilize the active conformation. The novel orientation of Hybrid domain presented in $\overrightarrow{IEF}$ set is unstable and would rotate back to the close state after the withdrawal of external forces for ELB or FAD. These results, as an opposite model, further confirm the close relationship among αI, βI, and Hybrid domains because the activation of the αI and βI

domains is not induced in this set compared with those in $\overrightarrow{EIF}$ and $\overrightarrow{EF}$ sets. Nevertheless, other conformational transmission modes may exist between the α- and β-subunits. For example, blood flow acting on β_2-integrin-expressed leukocytes or collision of flowing leukocytes to ICAM-1-expressed endothelium introduces the random fluctuation of β_2 integrin or β_2-integrin-ICAM-1 complex. These random fluctuations could trigger the instantaneous, diverse conformation changes of the β_2 integrin, finally resulting in distinct signal transduction mechanisms. In fact, the existence of the new conformation state with open headpieces and bent legs indicates the potential variety of conformational transmission for I-domain-containing integrins (3,45), even though the elaborative allosteric pathways are unclear. As a whole, this work elaborated the conformational dynamics of mechanically regulated outside-in activation of an I-domain-containing integrin and provided a, to our knowledge, new insight into understanding the cooperation between ELB and ILB and the roles of external force on the allosteric mechanisms of I-domain-containing integrin.

CONCLUSION

ILB is a prerequisite to initiate allosteric transmission and bear external forces. The αI domain opening state is featured as the stable intersubunit conformational transmission, with the downward movement and the lower half unfolding of α7-helix. A novel but unstable conformation of swingout of the β-subunit Hybrid domain is also proposed. Both external and internal bindings mutually support each other with significant reduction of binding time once one binds first.

SUPPORTING MATERIAL

Supporting Material can be found online at https://doi.org/10.1016/j.bpj. 2020.07.022.

AUTHOR CONTRIBUTIONS

D.M., S.L., and M.L. designed the research and wrote the article. D.M. performed all the simulations. X.Z. analyzed the data.

ACKNOWLEDGMENTS

REFERENCES

1. Sumagin, R., H. Prizant, …, I. H. Sarelius. 2010. LFA-1 and Mac-1 define characteristically different intralumenal crawling and emigration patterns for monocytes and neutrophils in situ. *J. Immunol.* 185:7057–7066.

2. Park, E. J., A. Peixoto, …, M. Shimaoka. 2010. Distinct roles for LFA-1 affinity regulation during T-cell adhesion, diapedesis, and interstitial migration in lymph nodes. *Blood.* 115:1572–1581.

3. Fan, Z., S. McArdle, …, K. Ley. 2016. Neutrophil recruitment limited by high-affinity bent β2 integrin binding ligand in cis. *Nat. Commun.* 7:12658.

4. Lee, J. O., P. Rieu, …, R. Liddington. 1995. Crystal structure of the A domain from the alpha subunit of integrin CR3 (CD11b/CD18). *Cell.* 80:631–638.

5. Shimaoka, M., T. Xiao, …, T. A. Springer. 2003. Structures of the alpha L I domain and its complex with ICAM-1 reveal a shape-shifting pathway for integrin regulation. *Cell.* 112:99–111.

6. Takagi, J., B. M. Petre, …, T. A. Springer. 2002. Global conformational rearrangements in integrin extracellular domains in outside-in and inside-out signaling. *Cell.* 110:599–611.

7. Su, Y., W. Xia, …, T. A. Springer. 2016. Relating conformation to function in integrin α5β1. *Proc. Natl. Acad. Sci. USA.* 113:E3872–E3881.

8. Chen, X., C. Xie, …, T. A. Springer. 2010. Requirement of open headpiece conformation for activation of leukocyte integrin alphaXbeta2. *Proc. Natl. Acad. Sci. USA.* 107:14727–14732.

9. Dong, X., N. E. Hudson, …, T. A. Springer. 2014. Structural determinants of integrin β-subunit specificity for latent TGF-β. *Nat. Struct. Mol. Biol.* 21:1091–1096.

10. Zhu, J., B. H. Luo, …, T. A. Springer. 2008. Structure of a complete integrin ectodomain in a physiologic resting state and activation and deactivation by applied forces. *Mol. Cell.* 32:849–861.

11. Cormier, A., M. G. Campbell, …, Y. Cheng. 2018. Cryo-EM structure of the αvβ8 integrin reveals a mechanism for stabilizing integrin extension. *Nat. Struct. Mol. Biol.* 25:698–704.

12. Welzenbach, K., U. Hommel, and G. Weitz-Schmidt. 2002. Small molecule inhibitors induce conformational changes in the I domain and the I-like domain of lymphocyte function-associated antigen-1. Molecular insights into integrin inhibition. *J. Biol. Chem.* 277:10590–10598.

13. Yang, W., M. Shimaoka, …, T. A. Springer. 2004. Intersubunit signal transmission in integrins by a receptor-like interaction with a pull spring. *Proc. Natl. Acad. Sci. USA.* 101:2906–2911.

14. Carreño, R., D. Li, …, G. B. Legge. 2008. A mechanism for antibody-mediated outside-in activation of LFA-1. *J. Biol. Chem.* 283:10642–10648.

15. Liu, J., T. Fu, …, J. Chen. 2014. The hydrophobic contacts between the center of the βI domain and the α1/α7 helices are crucial for the low-affinity state of integrin α4 β7. *FEBS J.* 281:2915–2926.

16. Zhang, C., J. Liu, …, J. Zhu. 2013. Modulation of integrin activation and signaling by α1/α1′-helix unbending at the junction. *J. Cell Sci.* 126:5735–5747.

17. Xie, C., J. Zhu, …, T. A. Springer. 2010. Structure of an integrin with an alphaI domain, complement receptor type 4. *EMBO J.* 29:666–679.

18. Sen, M., K. Yuki, and T. A. Springer. 2013. An internal ligand-bound, metastable state of a leukocyte integrin, αXβ2. *J. Cell Biol.* 203:629–642.

19. Sen, M., and T. A. Springer. 2016. Leukocyte integrin αLβ2 headpiece structures: the αI domain, the pocket for the internal ligand, and concerted movements of its loops. *Proc. Natl. Acad. Sci. USA.* 113:2940–2945.

20. Lee, J. O., L. A. Bankston, …, R. C. Liddington. 1995. Two conformations of the integrin A-domain (I-domain): a pathway for activation? *Structure.* 3:1333–1340.

21. Puklin-Faucher, E., M. Gao, …, V. Vogel. 2006. How the headpiece hinge angle is opened: new insights into the dynamics of integrin activation. *J. Cell Biol.* 175:349–360.

22. Xiao, T., J. Takagi, …, T. A. Springer. 2004. Structural basis for allostery in integrins and binding to fibrinogen-mimetic therapeutics. *Nature.* 432:59–67.

23. Wegener, K. L., A. W. Partridge, …, I. D. Campbell. 2007. Structural basis of integrin activation by talin. *Cell.* 128:171–182.

24. Li, H., Y. Deng, …, C. Yu. 2017. Structural basis of kindlin-mediated integrin recognition and activation. *Proc. Natl. Acad. Sci. USA.* 114:9349–9354.

25. Springer, T. A., J. Zhu, and T. Xiao. 2008. Structural basis for distinctive recognition of fibrinogen gammaC peptide by the platelet integrin alphaIIbbeta3. *J. Cell Biol.* 182:791–800.

26. Zhu, J., J. Zhu, and T. A. Springer. 2013. Complete integrin headpiece opening in eight steps. *J. Cell Biol.* 201:1053–1068.

27. Borst, A. J., Z. M. James, …, D. Veesler. 2017. The therapeutic antibody LM609 selectively inhibits ligand binding to human alphaVbeta3 integrin via steric hindrance. *Structure.* 25:1732–1739.e5.

28. Schürpf, T., and T. A. Springer. 2011. Regulation of integrin affinity on cell surfaces. *EMBO J.* 30:4712–4727.

29. Adair, B. D., J. P. Xiong, …, M. A. Arnaout. 2013. EM structure of the ectodomain of integrin CD11b/CD18 and localization of its ligand-binding site relative to the plasma membrane. *PLoS One.* 8:e57951.

30. Chen, X., T. D. Kim, …, T. A. Springer. 2007. Structural plasticity in Ig superfamily domain 4 of ICAM-1 mediates cell surface dimerization. *Proc. Natl. Acad. Sci. USA.* 104:15358–15363.

31. Mao, D., S. Lü, …, M. Long. 2011. Conformational stability analyses of alpha subunit I domain of LFA-1 and Mac-1. *PLoS One.* 6:e24188.

32. Humphrey, W., A. Dalke, and K. Schulten. 1996. VMD: visual molecular dynamics. *J. Mol. Graph.* 14:33–38, 27–28.

33. Roberts, E., J. Eargle, …, Z. Luthey-Schulten. 2006. MultiSeq: unifying sequence and structure data for evolutionary analysis. *BMC Bioinformatics.* 7:382.

34. Phillips, J. C., R. Braun, …, K. Schulten. 2005. Scalable molecular dynamics with NAMD. *J. Comput. Chem.* 26:1781–1802.

35. MacKerell, A. D., D. Bashford, …, M. Karplus. 1998. All-atom empirical potential for molecular modeling and dynamics studies of proteins. *J. Phys. Chem. B.* 102:3586–3616.

36. Zhang, X., L. Li, …, M. Long. 2018. Salt bridge interactions within the β_2 integrin α_7 helix mediate force-induced binding and shear resistance ability. *FEBS J.* 285:261–274.

37. Chen, W., J. Lou, …, C. Zhu. 2011. Molecular dynamics simulations of forced unbending of integrin $\alpha(v)\beta_3$. *PLoS Comput. Biol.* 7:e1001086.

38. Bidone, T. C., A. Polley, …, G. A. Voth. 2019. Coarse-grained simulation of full-length integrin activation. *Biophys. J.* 116:1000–1010.

39. Kulke, M., and W. Langel. 2020. Molecular dynamics simulations to the bidirectional adhesion signaling pathway of integrin $\alpha_V\beta_3$. *Proteins.* 88:679–688.

40. Nishida, N., C. Xie, …, T. A. Springer. 2006. Activation of leukocyte beta2 integrins by conversion from bent to extended conformations. *Immunity.* 25:583–594.

41. Weitz-Schmidt, G., T. Schürpf, and T. A. Springer. 2011. The C-terminal αI domain linker as a critical structural element in the conformational activation of αI integrins. *J. Biol. Chem.* 286:42115–42122.

42. Vorup-Jensen, T., C. Ostermeier, …, T. A. Springer. 2003. Structure and allosteric regulation of the alpha X beta 2 integrin I domain. *Proc. Natl. Acad. Sci. USA.* 100:1873–1878.

43. Wang, Z., A. M. M. Thinn, and J. Zhu. 2017. A pivotal role for a conserved bulky residue at the α1-helix of the αI integrin domain in ligand binding. *J. Biol. Chem.* 292:20756–20768.

44. Zhang, K., and J. Chen. 2012. The regulation of integrin function by divalent cations. *Cell Adhes. Migr.* 6:20–29.

45. Fan, Z., W. B. Kiosses, …, K. Ley. 2019. High-affinity bent beta2-integrin molecules in arresting neutrophils face each other through binding to ICAMs in cis. *Cell Rep.* 26:119–130.e5.